International Journal of Scientific Research and Engineering Development-– Volume 6 Issue 5, Sept-Oct 2023

Available at www.ijsred.com

RESEARCH ARTICLE OPEN ACCESS

Energy Management in Electric Vehicle Using Monarch Butterfly Optimization

R. Padma Priya *, Dr.C.Agees Kumar**

*(Department of Electrical and Electronics Engineering, Arunachala College of Engineering for women Manavilai, Vellichanthai.

Email: priya.badran20@gmail.com)

** (Associate Professor Department of Electrical and Electronics Engineering, Arunachala College of Engineering for women Manavilai, Vellichanthai.)

Email: ageesofficials@gmail.com)

----------**********----------

Abstract:

Hybrid electric vehicles (HEVs) are gaining popularity due to their significance in the transportation industry. The intelligent choice of the approach for managing energy not only enables the optimal energy distribution among the different sources, but it also lowers system utilisation, lengthens the life of the employed sources, and satisfies the energy demand that influences the independent operation of the electric vehicle (EV). The proposed vehicle's hybrid energy storage system (HESS) consists of three power sources: solar photovoltaic (PV), battery, and supercapacitor (SC), all of which are connected to the DC bus via DC-DC power converters. Solar PV serves as the primary source, with the other two serving as backup. The DC bus is then connected to a inverter, which powers the vehicle's electric motor. In this paper, a fuzzy logic-based nonlinear controller with monarch butterfly optimisation (MBO) for a PV-HEV hybrid energy storage system is created. Furthermore, a fuzzy logic-based energy management unit with the proposed control architecture has been deployed to reduce solar power consumption by utilising the maximum state of charge of the battery and supercapacitor. The converters connected to batteries and SCs are controlled by a current control. A proposed EMS architecture includes a load, batteries, SCs, and PV energy. SCs and reference current batteries are also included with this EMS. Simulation studies with different constants were conducted to demonstrate the effectiveness of the suggested control strategy.

Keywords **—Hybrid electric vehicles (HEVs), The hybrid energy storage system (HESS), monarch butterfly optimization (MBO), solar photovoltaic (PV), battery, supercapacitor (SC).**

----------**********----------

I. INTRODUCTION

The expansion in human migration has been accompanied by a significant increase in the global car population. Because of rising greenhouse gas emissions, depletion of oil supplies, and price volatili-ty, the world has focused on shifting its reliance from fossil fuels to renewable energy sources. The classic internal combustion engine (I.C.E) employed in transportation vehicles is a primary contributor to these greenhouse emissions. With these environmental concerns in mind, numerous vehicle manu-facturers such as Toyota, Volkswagen, Hyundai, and Ford are transitioning from traditional I.C.E-powered vehicles to electric vehicles (EVs). Although they may increase the capacity, safety, and fuel

efficiency of the transportation system, EV have grown in popularity in today's culture.

Electric vehicles that use both batteries and supercapacitors have piqued the interest of research-ers due to their unique power sharing capabilities. The HESS, which consists of batteries and super capacitors, is suggested on account of the unpredictable and variable load power needed for electric vehicle operation. The high-power density supercapacitor can be recharged and drained many times with a long cycle life and a quick response time, whereas a high-energy density battery cannot. The HESS makes full use of the advantages of the two complementary energy sources while making up for the shortcomings of the traditional single-energy storage system. In this thesis, the HESS nonlinear control approach and energy management strategy for electric vehicles are developed.

Because of the integration of several energy sources such as solar photovoltaic (PV),batter-ies, and super-capacitor (SC), these cars are usually referred to as Hybrid Electric cars (HEVs). One of these sources, the "Main Energy Source" (MES), is required to provide a longer drive cycle because of its high density of energy. Because of its reversibility and high energy density, the "Auxiliary Energy Source" (AES) is an additional kind that is in charge of meeting the load need during acceleration and may be refilled using regenerative braking energy.

Because of its high density of energy, the system under study includes solar PV as MES. There are no carbon emissions or noise pollution because it creates electricity by absorbing sunlight and converting that light energy into an electrical current. The combination of SC and batteries is em-ployed for AES because it can provide a balance of high power and high energy density. Because of its unidirectional power flow, the PV is inter-connected to the DC Bus via a DC/DC Boost converter, whereas the SC and batteries are connected to the DC Bus via a bi-directional boost converter and buck converter because to their reversibility in power flow.

To properly distribute load power among the pack of batteries and the supercapacitor, the EMS of an electric vehicle's energy storage system is being investigated. The supercapacitor supplies the high-frequency part of the load power variations when it varies frequently and violently, and the battery supplies the low-frequency portion of the load power fluctuation to protect the battery, lengthen its use-ful life, and minimise the variation of battery charging and discharging energy.

For the aforementioned three energy sources, several converter combinations and unique oper-ating topologies have been demonstrated. Another approach equips HEVs with several types of DC-DC converters, including fly-back converters and multi-device interleaved DC-DC converters. Each source has been explored in conjunction with its own independent power converter. A multiple con-verter architecture, in which each source has its own converter, has also been proposed, although it is expensive. A multi-input multi-output (MIMO) converter topology that is affordable has been demon-strated. However, it has been determined that the MIMO architecture is more challenging to operate and control than the previously stated design.

In the literature, linear control strategies have typically been used for such systems, ignoring the nonlinear characteristics of the DC-DC converters and sources of power. There have lately been devel-oped several nonlinear control schemes for battery and supercapacitor-based PV-HEVs. Similar to this, a Lyapunov function-based controller and parallel HESS modelling and control have been created for FHEV. An adaptive sliding mode control law for HESS has been created. The perturb and observe (P&O) approach using fuzzy logic controllers has been researched for PV and battery-based energy storage systems. Numerous systems' controllers have been built using backstepping and integral

back-stepping algorithms, but no energy management technique for achieving optimal power consumption among sources has been created. A hybrid electric car with fuzzy logic as the primary power source and a supercapacitor as an auxiliary source has been investigated.

The structure of the paper is described as follows: In section 2, the proposed system with mod-elling of each components is described. The energy management system for hybrid electric vehicle and optimization of such system is illustrated. Section 4 covers the simulation results of the proposed mod-el. Section 5 contains conclusion.

II. PROPOSED SYSTEM.

These cars are known as Hybrid Electric vehicle (HEVs) because to the existence of multiple energy sources such as solar photovoltaic (PV), batteries, and super-capacitors. Because of its high en-ergy density, one of these sources, termed as the "Main Energy Source," is required to provide a longer drive cycle. Because of its high energy density, solar PV is used as MES in the system under evalua-tion. There are no greenhouse gases or disturbances in the environment because it produces energy by absorbing sunlight and converting that ray of light into electricity. Because it can deliver an equal amount of high power and high energy density, AES uses a combination of SC and batteries. Due to its unidirectional power flow, the PV is connected to the DC Bus using a DC/DC Boost converter, whereas the SC and batteries are connected to the DC Bus using a bi-directional boost converter and buck converter because of their reversible power flow.

The system's electric circuitry includes a solar PV connected to a boost converter, a battery, and a supercapacitor coupled to their respective boost and buck converters. The traction motor of the vehicle is driven by a DC-AC converter, which is connected to the DC bus on the opposite side. A high-power density, a protracted operational life, and a reasonably high efficiency are suitable characteristics for the HESS. The HESS model depicted in Fig. 1 satisfies each condition.

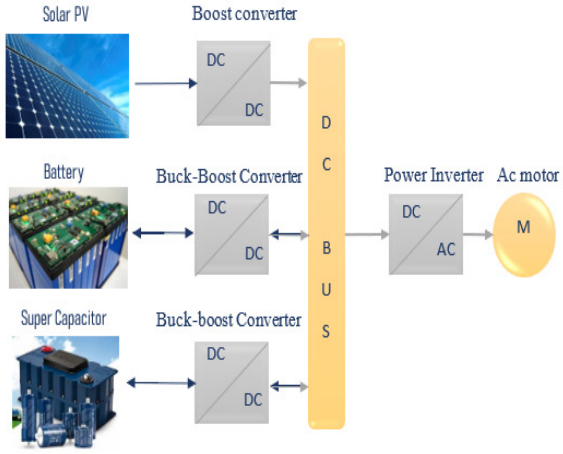

Fig. 1 Structure of proposed PV-SC-Battery based HEV

A. ***Solar PV modelling***

A detailed PV model is necessary to optimise the core design of a PV system by considering the effects of climate, irradiation ratios, thermal dissipation of Solar array, as well as the interconnection of series - parallel module to build an array. Figure 2 shows the circuitry of a photovoltaic cell. The section outlined by red dotted line represents the perfect PV cell, which acts as a Dc voltage source. In a standard method of the PV cell, the interface resistant and resistance value of a diode are mixed in series - parallel to imitate the PV cell's real behaviour. Using a single diode model, the analogous circuit of a PV cell is displayed in Fig 2.

A PV system is composed of numerous PV modules connected in series and parallel, respectively, to increase voltage and boost current. Owing to the presence of bypass diodes, the P-V characteristic curve in PSCs exhibits several peaks, also known as local and global maximum points. Bypass diodes placed in parallel with each PV module reduce the possibility of hot spots in PSCs, when the shadowed modules acts as a demand rather than providing power.

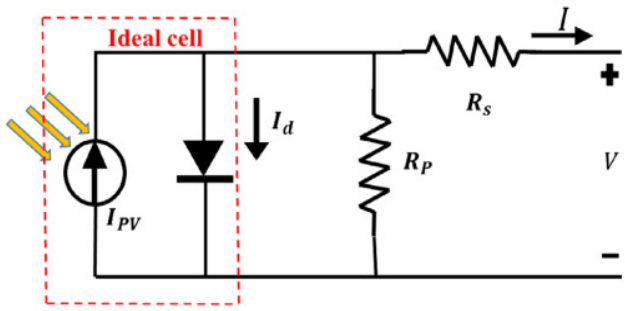

Fig 2. PV cell equivalent circuit single-diode model

The output in the form of current is given by Eq. (`1)

$$I = I_{pv} - I_0\left(exp\left(\frac{V+R_sI}{V_t\alpha}\right) - 1\right) - \frac{V+R_sI}{R_s} \qquad (1)$$

The following definitions pertain to the symbols used in the model:

I_{PV} :PV source current;

R_S :The total resistance caused by all the elements in the course of a current should be as minimal as possible;

R_P : to depict the leakage out across P-N junction, that should ideally be as wide as feasible;

I :difference between both the diode current ID and the photocurrent I_{PV}

When T is the temperature coefficient and G is the irradiation level, equations (2), (3), and (4) are used to calculate the PV cell current, saturation current, and thermal voltage.

$$I_{pv} = \left(I_{pv,n} + K_1(T - T_n)\right)\frac{G}{G_n} \qquad (2)$$

Saturation current is given as,

$$I_0 = \frac{(I_{SC}+K_1(T-T_n))}{\exp\left(V_{oc}+\frac{K_v(T-T_n)}{aV_t}\right)-1} (3)$$

Thermal voltage is given as,

$$V_t = \frac{N_sKT}{q} (4)$$

PV systems are made up of a grid of PV cells. Current I is improved by the parallel cell combination while voltage V is added by the series cell arrangement. The number of parallel cells is Np,whereas the number of series cells is Nm. Eq.(1) is transformed into Eq.(5).

$$I = N_pI_{pv} - N_pI_o(\exp\left(\frac{V+R_{seq}I}{N_MV_Ta}\right) - 1) - \frac{V+R_{seq}I}{R_{peq}} \qquad (5)$$

In order to regulate the voltage across the DC bus and in accordance with the load current, a unidirectional DC-DC boost converter was used because the power supply is not rechargeable. A single isolated gate bipolar transistor (IGBT) with a switch S_1, a high frequency inductor L_2 with an internal resistance R_1, and an output capacitance C_0 is used in this converter.

Table 1 Parameters specification of the solar array

Item	Specification
Maximum Power	150W
Module efficiency	11.7%
Open circuit Voltage	41.8 V
Short Circuit Current	505 A
Width	1250 mm
Length	1250 mm
Thickness	35 mm
Weight	15.5kg

B. ***Battery modelling***

The electrical circuit of this energy storage device is composed of a capacitor C and a current source. The battery's state of charge (SoC), a temporally dependent variable that can be written as:, controls how it charges and discharges.

$$SOC_{bat} = SOC_{bini} - \frac{1}{C_{cap}}\int_0^t I_{bat}dt \qquad (6)$$

where SOC_{bini} is the battery's initial SoC at t = 0 s and C_{cap} is the capacitor's capacity. A battery is a rechargeable power source that supplies power based on the load need. The battery is utilised as an AES in this suggested HESS. Because it permits electricity to flow in both directions for charging and discharging, a bi-directional DC-DC boost converter was used. This converter includes two IGBTs with switches S_2 and S_3, as well as an inductor L_2 with an internal resistance R_2.

Table 2 Parameter specification of a battery

Item	Specifications
Rated voltage	115V
Rated capacity	4.4 Ah
Number of cells	32
dimensions	417*304*135 mm
Power	15kW
Weight	14kg
Specific power	1071.4W/kg
Specific energy	36.14h/kg

C. ***Supercapacitor modelling***

A supercapacitor's (SC) operation resembles that of a battery in many ways. A capacitor C and a

series equivalent resistance R_s make up SC's circuitry. The SC's ability to charge and discharge depends on SoC, which has a temporal component and may be expressed as:

$$SOC_{sc} = SOC_{scini} - \frac{1}{C_{cap}} \int_0^t I_{sc} dt \quad (7)$$

where, SOC_{scini} is the SC's initial SoC at t = 0 s, andC_{cap} is the capacitor's capacity. It may possess positive as well as negative current values due to the charging and discharging stages. To make charging and discharging of the supercapacitor easier, a bidirectional DC-DC buck-boost converter was used. The SC uses plates and a dielectric to hold the charge. High power density, small size, and quicker charging are only a few benefits of a SC over a battery. However, there are also some disadvantages, including quick discharge, progressive voltage decline, and self-discharging. The battery's schematic also applies to the SC converter. Two IGBTs with switches S_4, inductor L_3andR_3 internal resistance are present.

Table 3. Parameter specification of SC module

Item	Specification
Rated energy	48 V
Rated capacitance	165 F
Number of cells	18
Maximum ESR	6.3m-ohm
Absolute maximum current	1900 A
Capacitance of individual cells	3000 F
Typical mass	13.5 kg
Useable specific power	3300 W/kg
Specific energy	3.9Wh/kg
Dimensions	418*194*126mm

a. Boost converter model for solar PV

The converter functions in two modes based on the position of switchS_1, which is an IGBT with a value range of 0 to 1. The subsequent equations can be found by using KVL:

$$\frac{di_{fc}}{dt} = -\frac{R_1}{L_1} i_{fc} + \frac{1}{L_1} v_{fc} - \frac{1-u_1}{L_1} v_{dc}$$
$$i_1 = (1-u_1) i_{fc} \quad (8)$$

where, $i_{pv}$and $v_{pv}$are solar PV current and voltage respectively, u_1 denotes the duty cycle of switch S_1, v_{dc}denotes the output voltage of DC bus and i_1 is the output current of boost converter.

b. Buck-boost converter model for battery

Charger mode and discharger mode are the two ways that a battery can operate. There has been use of a buck-boost converter with two switches, $S_3$and S_4. When the battery is discharged ($i_{batref} > 0$, S_3 is set to OFF, andS_2 can be in any position. In a similar manner, S_2 is set to OFF and S_3 can be in any position in charging mode ($i_{batref} > 0$), where i_{batref} is the desired reference value of battery current. The following formula represents the circuit model in the discharging mode:

$$\frac{di_{bat}}{dt} = -\frac{R_2}{L_2} i_{bat} + \frac{1}{L_2} v_{bat} - \frac{1-u_2}{L_2} v_{bat} \quad (9)$$

whereu_2 is the duty cycle of switch S_2, and v_{bat} and i_{bat} represent the battery's voltage and current, accordingly. The equations for the recharging mode are as follows:

$$\frac{di_{bat}}{dt} = -\frac{R_2}{L_2} i_{bat} + \frac{1}{L_2} v_{bat} - \frac{u_3}{L_2} v_{bat} \quad (10)$$

where u_3 represents the switch S_3 's duty cycle. Combining the aforementioned equations, the battery model looks like this:

$$u_{23} = \begin{cases} 1-u_2, & i_{batref} > 0 (discharging\ mode) \\ u_3, & i_{batref} < 0 (charging\ mode) \end{cases} \quad (11)$$

$$\frac{di_{bat}}{dt} = -\frac{R_2}{L_2} i_{bat} + \frac{1}{L_2} v_{bat} - \frac{u_{23}}{L_2} v_{bat} \quad (12)$$

$$i_2 = u_{23} i_{bat} \quad (13)$$

where, u_{23} and i_2 represent the converter's mean control input as well as output current, correspondingly.

c. Buck-boost converter model for supercapacitor

The procedure for both charging and discharging a SC is exactly the same as the one used for a battery, hence the equations for SC may be derived similarly as follows:

$$u_{45} = \begin{cases} 1-u_4, & i_{scref} > 0 (discharging\ mode) \\ u_5, & i_{scref} < 0 (charging\ mode) \end{cases} \quad (14)$$

$$\frac{di_{sc}}{dt} = -\frac{R_3}{L_3} i_{sc} + \frac{1}{L_3} v_{sc} - \frac{u_{45}}{L_3} v_{dc} \quad (15)$$

$$i_3 = u_{45} i_{sc} \quad (16)$$

where, The terms i_{scref} stand for the reference current of the SC, i_{sc}, v_{sc},i_3 for the output current of the converter, and u_{45} for the average control input of the converter, respectively.

The system's global mathematical model is provided below. Employing KCL as, allows for the expression of the voltage on the DC bus to be produced.

$$\frac{dv_{DC}}{dt} = \frac{1-u_1}{C} i_{fc} + \frac{u_{23}}{C} i_{bat} + \frac{u_{45}}{C} i_{SC} - \frac{1}{C} i_0 \quad (17)$$

where, $i_0$is the load current.

Table 4 component values of DC-DC converters

Parameter	Values
Inductors L_1, L_2 and L_3	3.3 mH
Inductor resistors R_1, R_2 and R_3	2.2 mH
Output capacitance C_0	1.66 F

III. FUZZY LOGIC-BASED ENERGY MANAGEMENT UNIT

System instability may result from control design without an effective energy management system if the distribution of electricity among sources fails to be sufficiently controlled under varying load demands. In order to generate reference currents for the battery and SC based on their SoC and load requirements, a fuzzy logic-based energy management unit (EMU) has been created, as shown in Fig. 3. This machine contains three inputs and two outputs, as well as 36 rules for determining the battery and SC reference currents under various load conditions.

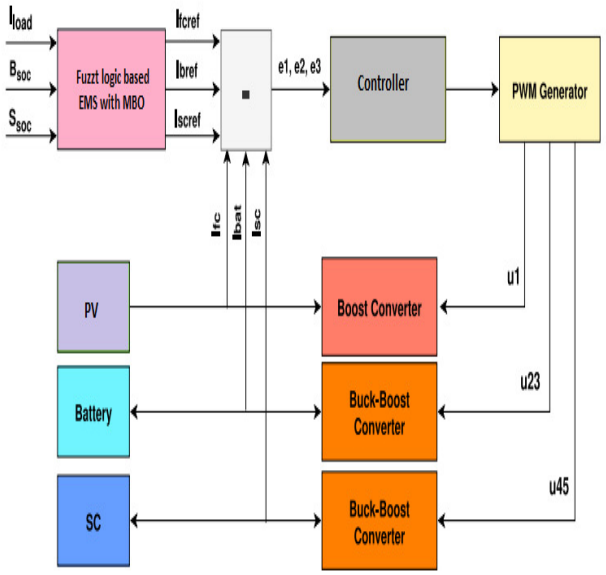

Fig 3. Control design and energy management of PV-HEV using fuzzy logic

The following has been implemented for the inputs, outputs, and associated membership functions:

• ***Input 1: Load current***

The load current, whose input has been separated into four membership functions—negative, low, medium, and high—determines the output from PV-HEV power sources. Because FC cannot operate while there is a negative load, battery and SC, depending on their SoC, collect the regenerative energy from the brakes and switch to charging mode.

• ***Input 2: State of charge of battery***

The SoC of the battery, which has been classified into three membership functions (low, medium, and high), determines how the battery acts as an auxiliary source and how much reference battery current is delivered by the EMU.

• ***Input 3: State of charge of supercapacitor***

The SoC of the SC, which supplies the electrical power peak during the initialization condition since PV is unable to meet the start-up and transient peak demands, determines the reference SC current that the EMU gives. SC instantly releases itself to give these modes an instant peak. Low, medium, and high membership tiers are available in the SoC of SC.

Table 5 Sample of designed EMU fuzzy rules for PVHEV

Rule no	I_{load}	SoC_{bat}	SoC_{sc}	I_{batref}	I_{scref}
1	Negative	Low	High	$charged_{fully}$	Idle
2	Negative	Medium	Low	$charged_{fully}$	$charged_{fully}$
3	Negative	High	Medium	$discharged_{fully}$	$charged_{fully}$
4	Low	Medium	High	$charged_{partially}$	Idle
5	Low	High	Low	$discharged_{partially}$	$charged_{partially}$
6	Low	Low	Medium	$discharged_{partially}$	idle
7	Medium	Low	High	idle	$discharged_{partially}$
8	Medium	Medium	Low	$discharged_{partially}$	Idle
9	Medium	High	Medium	$discharged_{fully}$	Idle
10	High	Low	High	Idle	$discharged_{fully}$
11	High	Medium	Low	$discharged_{fully}$	Idle
12	High	High	Medium	$discharged_{fully}$	$discharged_{fully}$

• ***Output 1: Battery reference current***

The battery reference current, which is the initial outcome from EMU, is determined by the battery's SoC and the required load current. It offers five membership options: $charged_{fully}$, $charged_{partially}$, idle, $discharged_{partially}$ and $discharged_{fully}$. Based on the load current and its SoC, the battery either charges, stays idle, or discharges itself.

• ***Output 2: SC reference current***

The SC reference current, which depends on the SoC of the SC and the required load current, is the second output from the EMU. It offers five

membership options:functions $\text{charged}_{\text{fully}}$, $\text{charged}_{\text{partially}}$, idle, $\text{discharged}_{\text{partially}}$ and $\text{discharged}_{\text{fully}}$.Depending on the load current and its SoC, the SC either charges, idles, or discharges itself. Table 6 displays an example of the rules that have been created for the EMU of FHEV.

This fuzzy logic-based EMU's 36 defined rules cover all of the functioning circumstances of the battery and supercapacitor under various load levels. The currents supplied by both the battery and supercapacitor under negative load conditions are shown by Rule No. 1 in the Table 5 samples. This hypothetical situation illustrates the state of the car once its brakes are activated. In this case, the SC is idle because of its high SoC, while the battery is charged via regenerative energy due to its low SoC. In accordance with Rule No. 5, in the low load condition, the battery partially discharges with the FC to satisfy the low load requirement, while the SC only partially charges itself to preserve the primary load generation balance because of its low SoC.

- SC is used to produce huge power fluctuations during prolonged load demands due to its high power density. Although it has an average SoC and a medium demand for load, the battery partially discharges itself to satisfy the load needed with FC while the SC is idle to prevent device degradation. Due to their shared high and medium SoCs, Rule No. 12 illustrates the high load requirement under when the battery and SC totally deplete in order to work with the FC.

A. ***Monarch Butterfly Optimization***

The original MBO method is straightforward and simple to implement. Subpopulation1 and suppopulation2 are two equal-sized subpopulations in MBO. It is worth noting that subpopulation1 consists of half of the individuals with the highest fitness value, whereas subpopulation2 consists of the remaining individuals. As a result, MBO employs two strategies: migration operator and butterfly adjusting operator. The two subpopulations are organised into an overall population following the first iteration, and the global optimum data is reserved. After that, the altered fitness value is used to split the total population into two subpopulations. To the point that the end-point condition is met, the cycle is repeated.

- ***Migration operator***

The positioning of other individuals in subpopulation1 or subpopulation2 affects the movement of individual i in subpopulation1, which can be countered by the adjusting ratio p. The migration operator's objective is to enhance interaction among the two subpopulations and inside each subpopulation1. In subpopulation 1, individual i's motion on the kth dimension can be expressed quantitatively as follows.

$$x_{i,k}^{t+1} = \begin{cases} x_{r1,k}^{t}, & if \;\; r \le p \\ x_{r2,k}^{t}, & else \end{cases} \qquad (18)$$

where the kth dimension ofx_i at generation t+1 is denoted by$x_{i,k}^{t+1}$. An integer index is used as the parameter r1, which is chosen at random from subpopulations 1 and 2, respectively. the parameter, where $r = rand * peri$, where peri is the migration time and rand is a random real value in the range [0, 1].

Butterfly adjusting operator

According to the adjusting ratio p and butterfly adjusting rate BAR for individual i in subpopulation2, the movement is expressed in terms of the current global best individual, a random individual in subpopulation2, and Lévy flight. When using a butterfly adjusting operator, three factors are taken into consideration: (1) Social model impact through progress towards the world's best. (2) The influence of other people on one's cognition by substituting a random person. (3) Using Lévy flight to broaden the search area and population variation. Using subpopulation2, the following function is used to create a new person:

$$x_{i,k}^{t+1} = \begin{cases} x_{best,k}^{t} & if\ rand \le p \\ x_{r3,k}^{t} & if\ rand > p \Delta rand \le BAR \\ x_{i,k}^{t} + \alpha \times (dx_k - 0.5) & if\ rand > p \Delta rand > BAR \end{cases} \qquad (19)$$

Where $x_{best,k}^{t}$ is the kth component of the current generational global optimum. The integral index r3 is one of the parameters, and it was chosen

at random from subpopulation 2. The butterfly adjustment rate is denoted by BAR. The weighting factor dx andα can be expressed as follows:

$$\alpha = S_{max}/t^2 \quad (20)$$

$$dx = Levy(x_i^t) \quad (21)$$

Where S_{max} is max walk step.

IV. RESULTS AND DISCUSSION

Using MATLAB/Simulink and a variety of load circumstances, the proposed/designed controller has been simulated and verified in this part. The proposed framework's primary goals are to regulate the DC bus voltage and to control the current flow by producing reference current for the power sources. Tables 1, 2, and 3 describe the specifications of the power sources, while Table 4 lists the parameters of the DC-DC converters employed in this study. According to the load needs and the controllers' tracking to the desired references, these settings were modified.

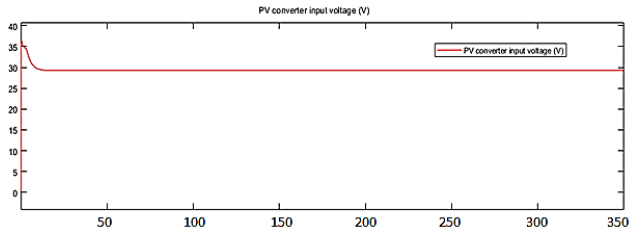

Fig 4. PV Converter Input Voltage

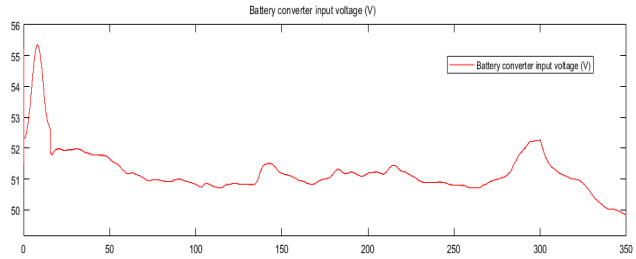

Fig 5. Battery Converter Input Voltage

The experimental time current and voltage time response of PV is shown in Figs. 6 and 7. At 20 seconds, the photovoltaic current in Fig. 4.4 reaches its maximum value of 55 A. Fig. 7. The PV voltage varies depending on the current applied to it. Additionally, it is evident that the PV behaves more slowly than the SC.

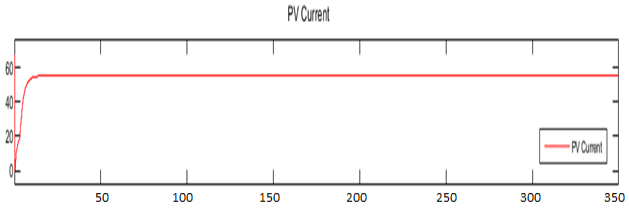

Fig 6. Output Current Waveform of Solar PV

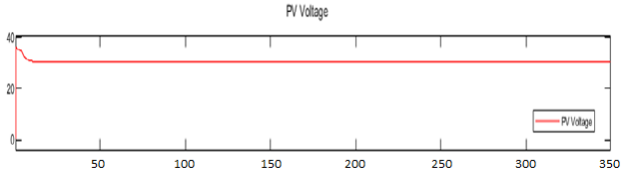

Fig 7 Output Voltage Waveform of Solar PV

Solar irradiance is the amount of energy that receives from the Sun in a form of electromagnetic waves that is measured in the range of wavelengths of the measuring device per unit area (watt per square metre, W/m2). Total Solar Irradiance is a unit of measurement for the solar power incident on the upper atmosphere of the Earth at all wavelengths. It is gauged perpendicular to the direction of the sun. The solar PV's irradiance waveform is shown in Fig. 8.

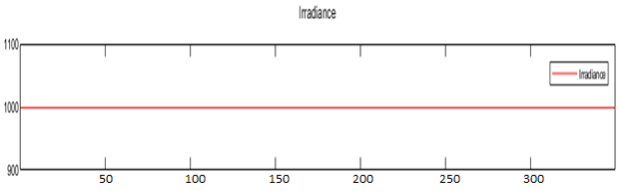

Fig 8. Irradiance waveform of solar PV

The absorption of solar radiation is the primary cause of air temperatures. They are influenced by a variety of variables, such as those of the environment, the oceans, and the land. The variation of solar radiation is the primary factor influencing climate, hence it is discussed first in this article. The temperature waveform of the solar PV is shown in Fig 9.

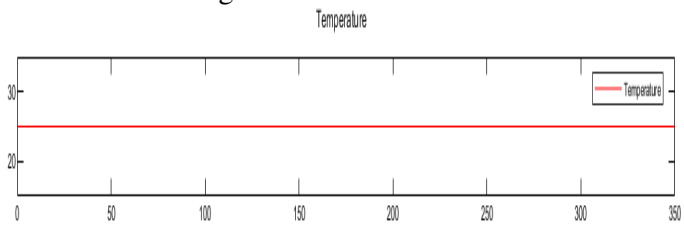

Fig 9 Temperature waveform of solar PV

The battery current and voltage are shown as curves in Figures 10 and 11. The battery current curve in Figure 10 demonstrates that it follows its set point with overshoots of around 15 A throughout the whole cycle. As seen in Fig. 11, the battery voltage varies between 51V and 52A, which is essentially constant.

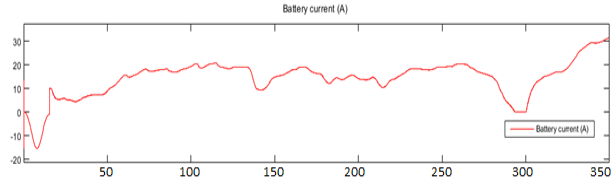

Fig 10. Output current waveform of battery

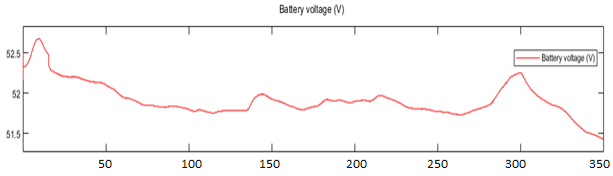

Fig 11. Output voltage waveform of battery

The fluctuation in the battery's SOC under various cycle circumstances and operation modes is shown in Fig. 12. The SOC performance in the operating mode is the most stable, and it can be maintained at a level of around 65%, which effectively realises the effect at the charge sustaining stage. On the basis of the battery's average SOC at the charge sustaining stage, the stability of the SOC under various operating modes is examined.

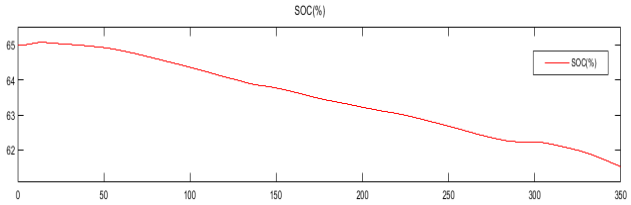

Fig 12 State of charge waveform of battery

The dynamic response of the SC current, voltage, and their references is shown in Figs. 13 and 14. The SC current accurately follows its reference at all times through Fig. 13. This demonstrates that the SC current tracks its reference almost flawlessly and without any error. Regarding the SC voltage in Fig. 14, the target SC voltage is 270V, and the SC voltage then returns to its starting value of 270V (keep in mind that this image has been zoomed, so the SC voltage variation is quite small).

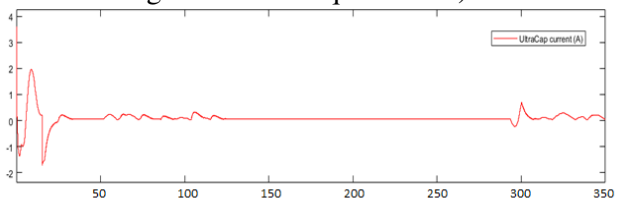

Fig 13 Output current waveform of supercapacitor

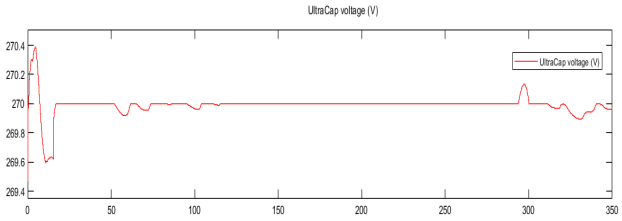

Fig 14 Output voltage waveform of supercapacitor

Fig 15 illustrates the output line voltage of the proposed system. From the figure we can witness that the voltage varies from -150 to 150, respectively. Fig 16. represents the output phase current of the proposed system. The phase current varies from -4A to 4A, respectively.

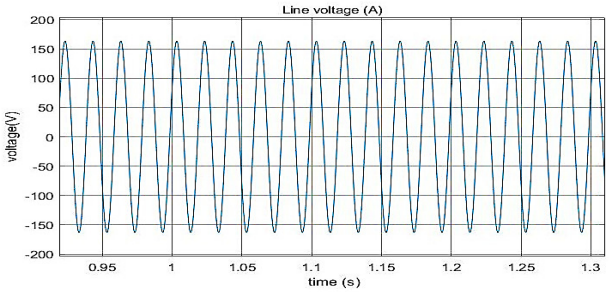

Fig 15. output line voltage

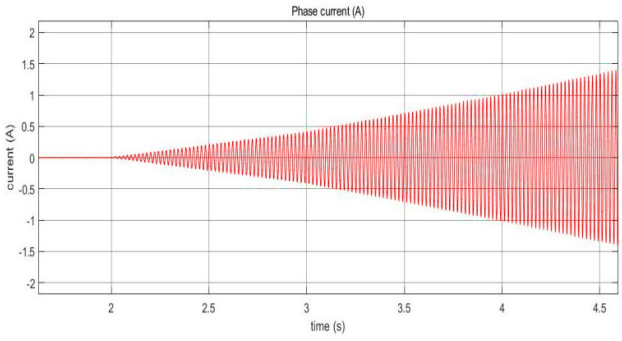

Fig 16. Output phase current

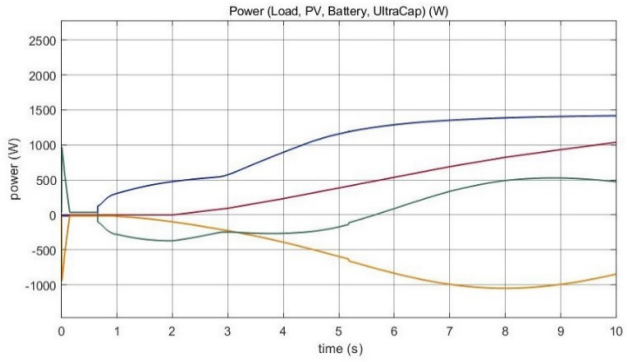

Fig 17. output power of load, PV, Battery, Supercapacitor

According to Fig. 17, for the entire working period, the Load powerP_L is equal to the sum of the PV power P_{PV} , battery power P_{BAT} , and SC powerP_{SC}. The PV power is consistently positive and behaves in a nearly seamless manner. Additionally, the traction power reaches 1400W, which, when taking into account the scale reduction of 1/60, corresponds to the maximum real traction power of 12 kW. Additionally, the battery may supplement the PV in supplying the load, such as during startup. The SC's sole purpose is to take in and/or supply the energy needed during sporadic phases.

V. CONCLUSION

In this work, a hybrid energy storage system made up of a battery and a supercapacitor was explored as well as solar PV as the main energy source. In order to create reference current for energy storage units depending on their state of charge and load requirements, a fuzzy logic-based energy management unit with MBO has been developed. A nonlinear controller based on fuzzy logic has been created for the PV-HEV hybrid energy storage system. The suggested framework was tested using the MATLAB/Simulink environment. To stabilise the DC bus voltage, a control strategy based on voltage command was introduced. A current control regulates the converters connected to batteries and SCs. It was suggested to use an EMS with batteries, SCs, PV energy, and load. SCs and reference current batteries are also available from this EMS.Simulation tests with various constants were conducted to show the efficiency of the suggested control approach. These hypothetical investigations proved the proposed EMS's capacity to transfer energy across diverse devices. Furthermore, it was discovered that SC integration reduced battery usage and removed peak current by comparing the SOC of batteries with various values of the filter constant. Indeed, decreasing battery SOC usage by increasing the filter constant.

ACKNOWLEDGMENT

This work was supported by Department of Electrical and Electronics Engineering, Arunachala College of Engineering for womenManavilai, Vellichanthai.

REFERENCES

[1] HuayanranZhou;YihongZhou;JunjieHu;GuangyaYang;DongliangXie; YushengXue;LarsNordström, 2021, "LSTM-based Energy Management for Electric Vehicle Charging in Commercial-building Prosumers" Journal of Modern Power Systems and Clean Energy, Vol. 9, No. 5.

[2] Arian Zahedmanesh;Kashem M. Muttaqi;DannySutanto, 2021, "A Cooperative Energy Management in a Virtual Energy Hub of an Electric Transportation System Powered by PV Generation and Energy Storage" IEEE Transactions on Transportation Electrification, Vol 7, No. 3, pp. 1123 – 1133.

[3] ChunhuaZheng;WeiminLi;Quan Liang, 2018, "An Energy Management Strategy of Hybrid Energy Storage Systems for Electric Vehicle Applications" IEEE Transactions on Sustainable Energy, Vol. 9, No. 4.

[4] Bo Zhao;XiangjinWang;DaLin;Madison M. Calvin;Julia C. Morgan;RuwenQin;Caisheng Wang, 2018, "Energy Management of Multiple Microgrids Based on a System of Systems Architecture" IEEE Transactions on Power Systems, Vol. 33, No. 6, pp. 6410 – 6421.

[5] XiangjunLi;Shangxing Wang, 2021, "Energy management and operational control methods for grid battery energy storage systems" CSEE Journal of Power and Energy Systems, Vol. 7, No. 5.

[6] HrvojeNovak;VinkoLešić;MarioVašak, 2019, "Hierarchical Model Predictive Control for Coordinat-ed Electric Railway Traction System Energy Management" IEEE Transactions on Intelligent Transpor-tation Systems, Vol. 20, No. 7, pp. 2715 – 2727.

[7] 1zhaoxi liu;QiuweiWu;MohammadShahidehpour;CanbingLi;ShaojunHuang;Wei Wei, 2019, "Transactive Real-Time Electric Vehicle Charging Management for Commercial Buildings With PV On-Site Generation" IEEE Transactions on Smart Grid, Vol. 10, No. 5, pp. 4939 – 4950.

[8] Hiroshi Kikusato;KoheiMori;ShinyaYoshizawa;YuFujimoto;HiroshiAsano;YasuhiroHayashi;AkihikoKawashima;ShinkichiInagaki;Tatsuya Suzuki, 2019, "Electric Vehicle Charge–Discharge Management for Utilization of Photovoltaic by Coordination Between Home and Grid En-ergyManagement Systems" IEEE Transactions on Smart Grid, Vol. 10, No. 3

[9] M Huan Chen;RuiXiong;ChengLin;Weixiang Shen, 2021, "Model predictive control based real-time energy management for hybrid energy storage system" CSEE Journal of Power and Energy Systems, Vol. 7, No. 4

[10] SohaibRafique;Mohammad Jahangir Hossain; Mohammad Sohrab Hasan Nizami; Usama Bin Irshad; Subhas Chandra Mukhopadhyay, 2021, "Energy Management Systems for Residential Buildings With

Electric Vehicles and Distributed Energy Resources" IEEE Access, Vol. 9.

[11] Kyaw Hein;YanXu;GaryWilson;Amit K Gupta, 2021, "Coordinated Optimal Voyage Planning and Energy Management of All-Electric Ship With Hybrid Energy Storage System" IEEE Transactions on Power Systems, Vol. 36, No. 3,pp. 2355 – 2365.

[12] NingyuanGuo;XudongZhang;YuanZou;BasilioLenzo;GuodongDu;Tao Zhang, 2021, "A Supervi-sory Control Strategy of Distributed Drive Electric Vehicles for Coordinating Handling, Lateral Stabil-ity, and Energy Efficiency" IEEE Transactions on Transportation Electrification, Vol. 7, No. 4, pp. 2488 – 2504.

[13] ChristoforosChatzikomis;AldoSorniotti;PatrickGruber;MattiaZanchetta ;DanWillans;Bryn Bal-combe, 2018, "Comparison of Path Tracking and Torque-Vectoring Controllers for Autonomous Elec-tricVehicles"IEEE Transactions on Intelligent Vehicles, Vol. 3, No. 4.

[14] Bo Wang;PaymanDehghanian;ShiyuanWang;MassimoMitolo, 2019 "Electrical Safety Considera-tions in Large-Scale Electric Vehicle Charging Stations" IEEE Transactions on Industry Applications, Vol. 55, No. 6, pp. 6603 – 6612.

[15] Amir Rezaei;Jeffrey B. Burl;MohammadRezaei;Bin Zhou, 2018, "Catch Energy Saving Opportunity in Charge-Depletion Mode, a Real-Time Controller for Plug-In Hybrid Electric Vehicles" IEEE Trans-actions on Vehicular Technology, Vol. 67, No. 11, pp. 11234 – 11237.

